Design and Development of a High Pumping Frequency Piezoelectric–Hydraulic Hybrid Actuator

JAYANT SIROHI* AND INDERJIT CHOPRA

Department of Aerospace Engineering, Alfred Gessow Rotorcraft Center, University of Maryland, College Park, MD 20742, USA

ABSTRACT: This paper describes the design and development of a piezoelectric–hydraulic hybrid actuator operating at a high pumping frequency. The actuator is envisaged as a potential actuator for a trailing edge flap on a full scale smart rotor system. While recent research efforts based on the same concept have investigated actuators with large piezoelectric stacks operating at a relatively low pumping frequency, the goal of the present work is to investigate the behavior of the actuator at a low volumetric displacement and high pumping frequency. Preliminary design of the actuator system is carried out, and the dependence of the performance of the actuator on various system parameters is identified. This enables the optimum selection of geometric parameters and piezostack characteristics for a given external load. Challenges to achieving high pumping frequencies were identified and solutions were implemented. The actuator was driven by two piezostacks, of a total length of 36 mm and cross-sectional area 100 mm^2. The actuator was tested up to a pumping frequency of 1 kHz, developing a maximum no-load velocity of 1.2 in/s and a blocked force of 35 lb in the unidirectional output mode. Bidirectional output performance was also measured, by incorporating a 4-way valve in the hydraulic circuit. At a frequency of 5 Hz, a no-load output displacement with an amplitude 32 mils was measured.

INTRODUCTION

THE piezoelectric–hydraulic hybrid actuator is a device based on the frequency rectification principle, resulting in actuation at a large force with a theoretically unlimited stroke. The device consists of a pump driven by piezoelectric stacks, that pressurizes a hydraulic fluid. The fluid is then utilized to transmit the power to an output hydraulic cylinder. This results in a localized, self-contained actuation system that combines the advantages of the power transmission flexibility of hydraulics and the high energy density of piezoelectric stacks. In subsequent discussions, the entire piezoelectric-hydraulic hybrid device will be refered to as the actuator.

Recently, several actuator systems based on the concept of hybrid actuation are under development. Mauck et al. (2000, 2001) investigated a system consisting of a pump driven by a high voltage piezostack of length 10.2 cm and cross-sectional area 1.9 cm × 1.9 cm. Several versions of designs have been investigated, with accumulators incorporated into later designs. The final device achieved a blocked force of 61 lb and an output actuator velocity of 7 cm/s. The large current requirements and heating of the piezostack limited the pumping frequency of the system to 60 Hz. Nasser et al. (2000) presented a piezohydraulic actuation system that is driven by a piezostack with a free stroke of 100 μm. The system was operated at pumping frequencies of the order of 10 Hz. A magnetostrictive water pump was developed by Gerver et al. (1998), that operates at a relatively low pressure, of the order of 5 psi, and makes use of an additional hydraulic stroke amplification scheme to increase the flow rate. A flow rate of 15 mL/s at an output pressure of 5 psi has been reported. Konishi et al. (1993, 1994) have developed a piezoelectric–hydraulic hybrid actuator using a piezostack of length 55.5 mm and diameter 22 mm. The operating voltage of this piezostack is −100 V to +500 V and its free strain and blocked force are 60 μm and 10.8 kN respectively. This piezoelectric pump was excited at 300 Hz and delivered an output power of approximately 34 W. In this system, cooling water was used to limit the maximum temperature of the piezostacks.

A common feature of the above research efforts is that the required volumetric flow rate of the pump is obtained by using piezostacks of large length, limited to relatively low pumping frequencies. While this is sufficient as a proof of concept, it does not completely utilize the large bandwidth of the piezostacks. By operating the piezostacks at higher frequencies, the power density of the device can be increased. Additionally, it is important to

*Author to whom correspondence should be addressed.
E-mail: sirohij@eng.umd.edu

1045-389X/03/03 0135–13 $10.00/0 DOI: 10.1177/1045389X03031063

eliminate accumulators and external cooling systems in order to achieve a high power density of the device.

In the present work, the development of a piezoelectric–hydraulic hybrid actuation system is described, with its design focused on operation at a high pumping frequency, with a stroke of approximately 20 μm. It should be noted that the present prototype system is intended primarily as an experimental setup to validate theoretical predictions with measurements. Hence, while the present setup is not designed to be lightweight or compact, it incorporates all the features that would be desirable for a high power density in the final design, such as the absence of accumulators in the hydraulic circuit. Specifically, the actuator is envisaged as a potential self-contained trailing edge flap actuator on a full scale smart rotor. At this point, it is worth emphasizing that in such an application, power density, both in terms of power output per unit weight, and power output per unit volume of the actuator, should be as high as possible.

BASIC CONCEPT AND CONSTRUCTION

A schematic of the piezoelectric pump coupled to an output hydraulic cylinder is shown in Figure 1(a). In order to meet the requirements of a trailing edge flap on a section of a full scale MD900 rotor blade (Lee and Chopra, 2001), nominal output specifications are shown in Figure 1(b). An exploded view of the piezoelectric pump is shown in Figure 2(a). The piezostack assembly consists of two commercially available low voltage piezostacks (model P-804.10, Physik Instrumente (1997)), that are bonded together, end to end. The piezostack assembly is 36 mm long and has a square cross section with each side of 10 mm. A detailed description of the construction of the piezoelectric pump can be found in other publications (Sirohi et al., 2001, 2002).

The first prototype was fabricated out of C-1018 steel. However, in order to save weight, the final design could be fabricated out of aluminum. The assembled piezo-

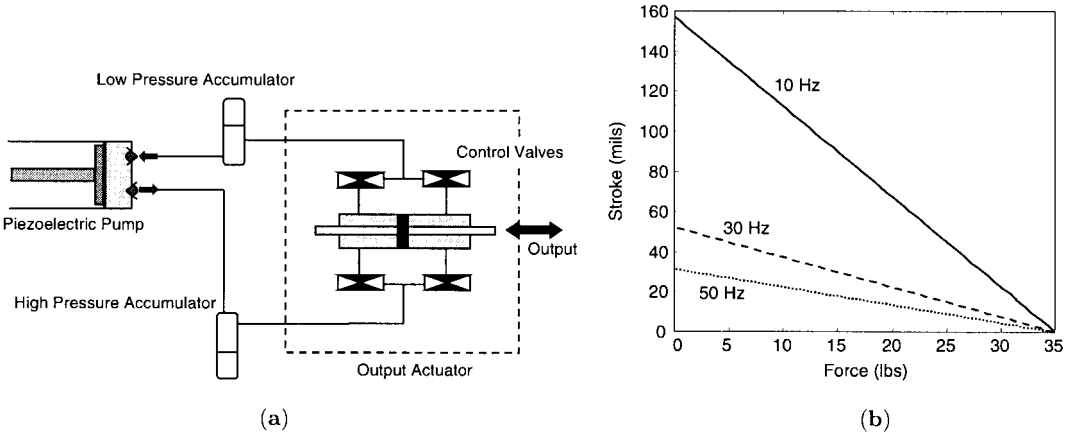

Figure 1. *Piezoelectric-hydraulic hybrid actuator: (a) Schematic; (b) Normal output design goals.*

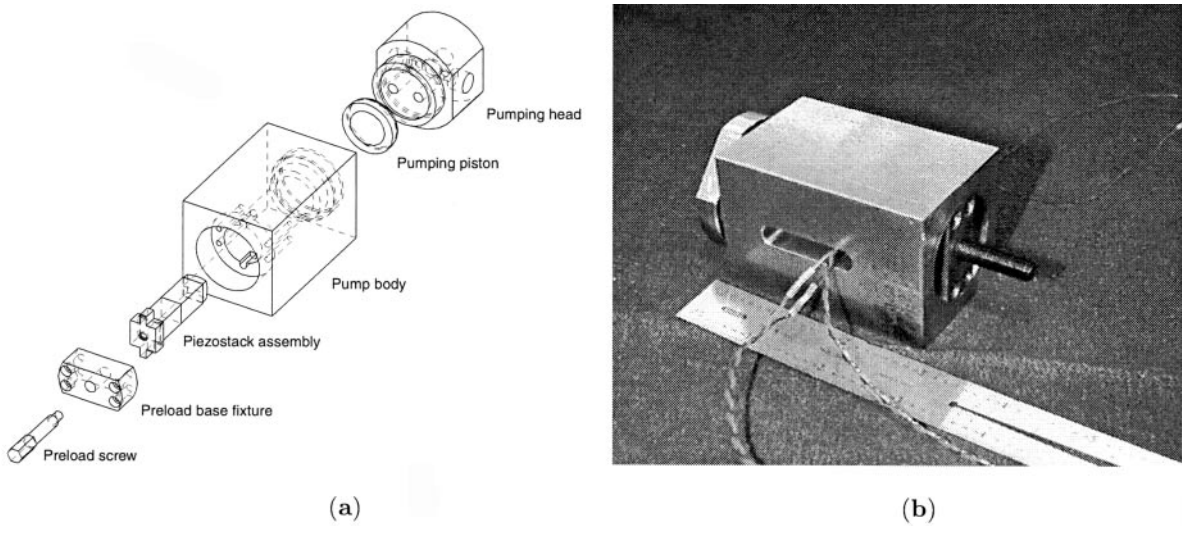

Figure 2. *First prototype piezoelectric-hydraulic pump: (a) Exploded view; (b) First assembled prototype*

electric pump is shown in Figure 2(b). The overall length of the entire piezoelectric pump assembly is under 4″ and it has a square cross section with each side of length 1.5″. A list of all the important parameters of the current design is shown in Table 1. The piezostack data are applicable for each piezostack (Lee and Chopra, 2001).

A simplified diagram of the working cycle of the piezoelectric pump is shown in Figure 3(a). The compression stroke, OB, has a slope less than 90° due to the finite stiffness of the working fluid. The limits of operation of the device are defined by the points B and C. The point B is the point of intersection of the fluid stiffness line and the piezostack load line. At this point, all the deformation of the piezostack goes into compression of the fluid in the pumping chamber. Hence, the net work output of the device is zero, and this condition is the output blocked condition. The corresponding force at the output hydraulic actuator is the blocked force of the device. At point C, the only force on the piezostacks is due to the required cracking pressure of the check valves. Once this is overcome, the fluid flows freely through the circuit. At this point, the maximum flow rate, or no-load flow rate of the piezostack pump is achieved. The output work of the device is however, zero, as the output load in this condition is zero. Maximum work output of the device is achieved at an intermediate point, that can be determined from a trade-off study as described below.

Table 1. Prototype device parameters.

Piezostack – Model P-804.10	
Number of piezostacks	2
Length	0.3937 in.
Width	0.3937 in.
Height	0.7087 in.
Blocked force	1133 lbs
Free displacement	≈ 0.5 mil
Operating voltage	0–100 V
Capacitance	≈ 7 μF
Hydraulic fluid – MIL-H-5606F	
Density	859 gm/cc
Kinematic viscosity	15 centistokes
Reference bulk modulus β_{ref}	2,60,000 psi
Pumping chamber	
Diameter	1 in.
Height	0.050 in.
Output actuator – double rod	
Bore diameter	0.5 in.
Shaft diameter	0.25 in.
Stroke	2 in.

PRELIMINARY SIZING CONSIDERATIONS

The dimensions of the first prototype were chosen based on output flow requirements and ease of manufacturing. Note that this prototype was intended primarily as a proof of concept. However, for the final design, the geometrical parameters as well as piezostack characteristics could be chosen in order to obtain the maximum work output from the actuator.

The performance of the actuator is highly sensitive to the dimensions of both the pumping chamber and the output hydraulic cylinder. The viscosity of the fluid, diameter of the tubing, and the modulus of elasticity of the tubing material are also important for the frictional losses that occur in the device as well as for its frequency response. However, for an initial design, it is convenient to neglect any frequency dynamics of the system, and assume a constant response at all pumping frequencies. As a result of this quasi-static pumping assumption, the volumetric flow rate of the pump, Q, at any given pumping frequency is equal to the product of the volumetric displacement of the pump per cycle, Δ_{pump} and the pumping frequency f_{pump}.

$$Q = \Delta_{\text{pump}} f_{\text{pump}} \tag{1}$$

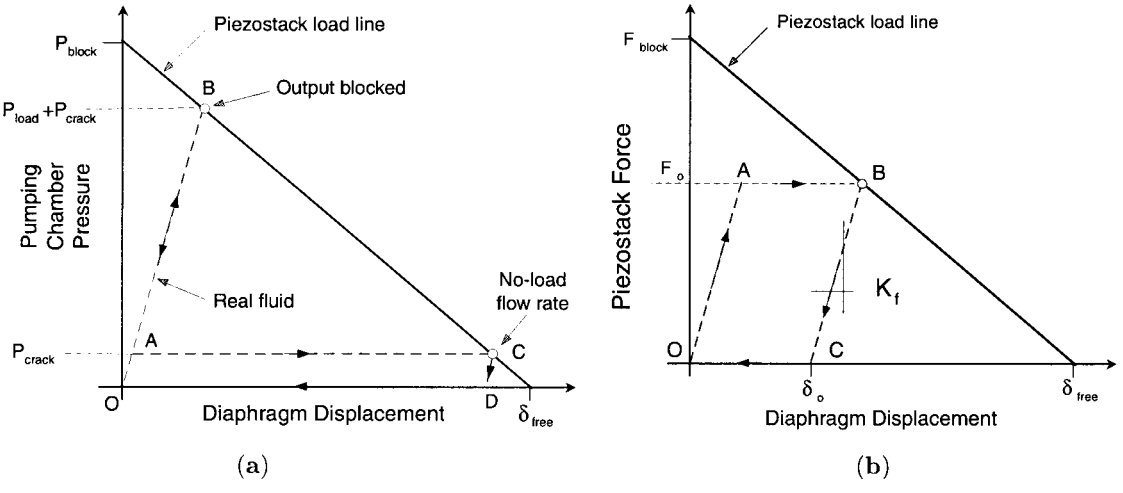

Figure 3. *Typical pumping cycles for a real working fluid: (a) Limits of operation; (b) Load-line analysis.*

The large flexibility in trading off force and stroke afforded by the use of hydraulics results in many possible combinations of pumping chamber and output cylinder dimensions. The final design is therefore very dependent on the output requirements of the device. Due to this strong coupling between the pump and output cylinder, all subsequent discussions of the performance of the actuator will be with respect to its force and stroke, as opposed to the pressure and flow rate generated by the pump.

Since the ultimate goal is to maximize output power density for a device of known external dimensions, the output power is considered to be the primary performance metric. The major variables on which the power output depends are:

- Pumping chamber diameter, d_{cham}
- Output cylinder diameter, d_{out}
- Pumping chamber height, Δ_{gap}
- Piezostack characteristics: Blocked force F_{block} and Free displacement δ_{free}
- Fluid compressibility, β

A piezostack which is known to have a high energy density (Lee and Chopra, 2001), was chosen to drive the first prototype pump. Hence the piezostack characteristics are assumed to be constant for this trade-off study. Similarly, the fluid compressibility is also assumed constant, because a low viscosity standard hydraulic oil, MIL-H-5606F was chosen as the working fluid.

Work Output Per Cycle: Load-line Analysis

As a result of the quasi-static pumping assumption (Equation (1)), to maximize the output power, it is sufficient to maximize the work done by the device per pumping cycle. This is given by the area OABCO in Figure 3(b), which outlines a typical pumping cycle.

The work done per cycle is given by

$$\Delta W_{\text{cyc}} = F_{\text{o}}\delta_{\text{o}} \tag{2}$$

The equation of the piezostack load line is given by

$$\delta = \delta_{\text{free}}\left(1 - \frac{F}{F_{\text{block}}}\right) \tag{3}$$

In order to calculate the area under the curve, it is necessary to derive expressions for the locations of the points A, B and C. This involves calculating the fluid stiffness K_{f}. An analysis of the stiffness of each constituent of the hydraulic circuit has been described in a previous study (Sirohi and Chopra, 2001). Comparing the relative magnitudes of the above stiffnesses for a typical set of system parameters, it can be seen that the stiffness of the accumulators is small compared to the large stiffness of the fluid and tubing. The diaphragm stiffness is approximately 10% of the piezostack stiffness in the current design. As a result of this, the fluid and tubing can be considered rigid, the accumulator stiffness can be ignored, and the system can be approximated to be a piezostack working against the load alone.

Work Done Per Cycle: Calculation of Operating Points

In the analysis, an effective load–force curve of the piezostack is used. This is obtained by scaling the original load line to account for the decrease in free stroke and block force of the piezostack–diaphragm assembly as a result of the diaphragm stiffness.

From Figure 3(b) and Equation (3),

$$\delta_{\text{o}} = \delta_{\text{free}} - F_{\text{o}}\left[\frac{1}{K_{\text{p}}} + \frac{1}{K_{\text{f}}}\right] \tag{4}$$

where K_{f} is the stiffness of the column of fluid in the pumping chamber and K_{p} is the stiffness of the piezostack. Defining an effective stiffness, K_{eff}

$$\delta_{\text{o}} = \delta_{\text{free}} - \frac{F_{\text{o}}}{K_{\text{eff}}} \tag{5}$$

It can be seen that the effective stiffness is obtained by a series combination of the piezostack and fluid stiffnesses. From Equations (5) and (2), the work output of the device per cycle is

$$\Delta W_{\text{cyc}} = F_{\text{o}}\left[\delta_{\text{free}} - \frac{F_{\text{o}}}{K_{\text{eff}}}\right] \tag{6}$$

This work is expressed in terms of pressure and displacement inside the pumping chamber. Figure 4 shows a schematic of the fluid column between the pumping chamber and the output actuator. The pumping chamber has a cross-sectional area A_{p} and a displacement δ_{p}, while the output actuator has a cross-sectional area A_{out} and a displacement δ_{out}. The area ratio is given by

$$A_{\text{R}} = \frac{A_{\text{out}}}{A_{\text{p}}} \tag{7}$$

The work output per cycle can be rewritten in terms of the force and displacement of the output actuator

$$\Delta W_{\text{cyc}} = \frac{F_{\text{out}}}{A_{\text{R}}}\left[\delta_{\text{free}} - \frac{F_{\text{out}}}{A_{\text{R}}K_{\text{eff}}}\right] \tag{8}$$

The stiffness of fluid in the pumping chamber can be derived to be

$$K_f = \beta \frac{A_p}{\Delta_{gap}} \tag{9}$$

For given working fluid, β is fixed, and A_p may be constrained by the overall size. In such a case, the only parameter which the designer is free to choose is the pumping chamber height, Δ_{gap}. In order to increase the power output of the device, it is desirable to maximize the stiffness of the fluid in the pumping chamber. This can be accomplished by either increasing the pumping chamber diameter or decreasing the pumping chamber height. However, if there are no other geometrical restrictions, it is more effective to increase the pumping chamber diameter than the height, because the fluid stiffness depends on the square of the diameter and is inversely proportional to the height. Substituting the expression for fluid stiffness back in Equation (8), the expression for output work per cycle is

$$\Delta W_{cyc} = \frac{F_{out}}{A_R}\delta_{free} - \frac{F_{out}^2}{A_R^2 K_p} - \frac{F_{out}^2 \Delta_{gap}}{A_R^2 \beta A_p} \tag{10}$$

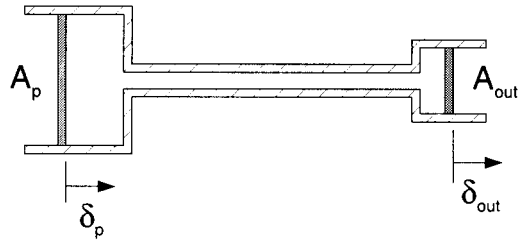

Figure 4. *Fluid line between pumping chamber and output actuator.*

Maximum Output Work

The dimensions of the output actuator are fixed by overall geometric constraints; a commercially available 0.5″ bore hydraulic actuator was chosen for the present device. This fixes the value of A_{out} and the only parameters that remain to be fixed are the diameter and height of the pumping chamber. It should be noted here that although maximum work output is the primary goal of the device, the application may dictate a certain displacement requirement at a certain bandwidth (Figure 1(a)). This requirement directly translates into the flow rate of the piezoelectric pump. Therefore, in addition to sizing the parameters of the device for maximum per cycle output work, the constraint of achieving the required output displacement must also be included in the design process.

Plots of the variation of output work with A_{out} and Δ_{gap} are shown in Figure 5. In Figure 5(a), the work output per cycle is plotted as a function of pumping chamber diameter for various output loads, with a pumping chamber height of 0.05″. The maximum work output per cycle is achieved at a certain value of pumping chamber diameter, and this maximum decreases with output load. Figure 5(b) shows the work output per cycle as a function of pumping chamber height, for a pumping chamber diameter of 1″. The maximum work output increases monotonically (at a slower rate) with decreasing pumping chamber height. This is to be expected as a smaller pumping chamber height increases the stiffness of the fluid and essentially provides a direct energy transfer to the output load. As this function has no extremum, a value of pumping chamber height between 0.02 and 0.05″ can be chosen depending on other factors such as

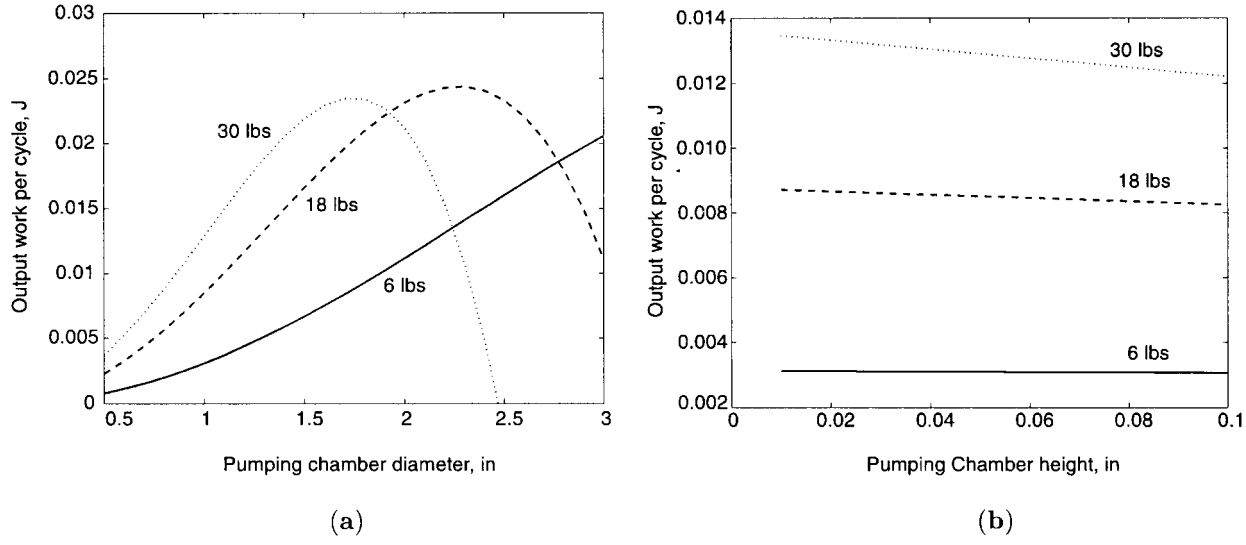

Figure 5. *Dependence of work output per cycle on pumping chamber geometry: (a) Work output as a function of pumping chamber diameter, $\Delta_{gap} = 0.05''$; (b) Work output as a function of pumping chamber height, $d_{cham} = 1''$.*

machinability and clearances. For the present proof of concept experimental actuator, the diameter of the pumping chamber was set at 1″ and the height of the pumping chamber was chosen as 0.05″.

The conditions for maximum output work per cycle can be obtained by differentiating Equation (10) with respect to the two parameters A_p and Δ_{gap}

$$\frac{\partial(\Delta W_{cyc})}{\partial A_p} \Rightarrow A_p = F_{block}\frac{A_{out}}{2F_{out}} - \Delta_{gap}\frac{K_p}{2\beta} \qquad (11)$$

If $\beta \to \infty$ in the above equation, the value of A_p reduces to an impedance matched condition, i.e., at the midpoint of the piezostack load line. This is as expected, since the maximum power output is known to occur at an impedance matched condition.

Based on the above discussion, taking into consideration any geometric constraints on the overall size of the device, an optimum pump geometry can be arrived at for a given output load. The fluid compressibility, which is a key parameter on which the power output of the device depends, can be very different from the reference value specified in the data sheet. The actual compressibility depends on several factors, like the system bias pressure and the amount of air entrained, and can be as low as 10% of the reference value (McCloy and Martin, 1980). This can have a significant effect on the output performance. It should be noted that the reference fluid bulk modulus is specified at 2500 psi, with no entrained air. The actual fluid bulk modulus is given by (The Lee Company, 1997)

$$\beta_{fluid} = E_p \times E_a \times \beta_{ref} \qquad (12)$$

where E_p and E_a are the correction factors for bias pressure and entrained air, and β_{ref} is the reference fluid bulk modulus, which for the current fluid is given as 260,000 Psi (Table 1). For the current system bias pressure of 50 psi, $E_p = 0.9$. The fraction of entrained air is assumed to be 1%, which is not an uncommon value for hydraulic systems. For this amount of entrained air, $E_a = 0.1$. It can be seen that the entrained air has a strong influence on the effective fluid bulk modulus. Substituting these values into Equation (12), the effective fluid bulk modulus is obtained as

$$\beta_{fluid} = 0.9 \times 0.1 \times \beta_{ref} = 23,400\,\text{psi} = 0.16\,\text{GPa} \qquad (13)$$

PERFORMANCE ESTIMATES

In order to obtain an approximate estimate of the blocked force of the device and the no-load cylinder velocity, a quick calculation can be performed assuming quasi-steady pumping. From Figure 3(a) and (b), the blocked force, or the maximum output force of the device F_{max} is obtained when $\delta_o = 0$. Applying this condition to Equation (4) leads to

$$F_{max} = \frac{\delta_{free}}{(1/K_p) + (1/K_f)} \qquad (14)$$

The value of K_f for the present results can be calculated using Equation (9). After substituting these numbers in the above equation, the estimated $F_{max} = 30.7$ lb.

To estimate the no-load cylinder velocity, based on a measured piston deflection of 0.8 mils, and given the device geometry in Table 1, the output swept volume per cycle is 0.6283×10^{-3} in^3. This is the same as the flow into the output hydraulic actuator, which gives, for a pumping frequency of 300 Hz, a no-load cylinder velocity of 1.2797 in/s. It should be noted that since the above estimate neglects fluid compressibility and flow resistance, this estimate represents an upper bound of the achievable no-load cylinder velocity.

HIGH PUMPING FREQUENCY OPERATION

While the operation of the system is relatively straightforward at low pumping frequencies, several challenges exist to achieve higher pumping frequencies. These are:

- Frequency response of the passive check valves
- Self-heating of the piezostacks
- Electrical power delivery to the piezostacks

While the self-heating of the piezostacks and the electrical power delivery issues limit the maximum possible pumping frequency, the frequency response of the passive check valves and the dynamics of the hydraulic circuit reduce the pumping efficiency at higher pumping frequencies. The above issues are addressed in the present work, and the frequency response of the hydraulic circuit is currently under investigation.

Frequency Response of the Passive Check Valves

The check valves installed in the first prototype piezoelectric pump were commercially available ball type check valves (The Lee Company, 1997). On examining the pumping chamber pressure traces, it was inferred that the dynamics of the check valves became significant at frequencies around 150 Hz (Sirohi and Chopra, 2002). Additionally, previous experiments measuring the flow rate of the pump indicated a peak in the flow rate between pumping frequencies of

100–200 Hz. Therefore, in the second prototype of the pump, the original check valves were replaced with higher natural frequency reed valves, that were designed and fabricated in-house. A cross-sectional view of the reed valves is shown in Figure 6. The theoretical resonant frequency of the reed valves is approximately 3 kHz; however, the actual resonant frequency is expected to be lower as the solder joint at the base of the reed does not provide an ideal clamped boundary condition. In subsequent discussions, the original check valves will be referred to as Type I valves and the valves fabricated in-house will be referred to as Type II valves.

Self-heating of the Piezostacks

Piezostack self-heating is a major factor limiting the maximum excitation frequency of the piezostacks. A detailed discussion of the causes of piezostack heating and its quantification was presented in a previous work (Sirohi and Chopra, 2001).

A simple way to prevent the piezostacks from overheating is to dissipate as much of the heat as possible through conduction from the piezostacks to the pump body, which acts as a large thermal sink. The main issue is to provide a heat transfer path from the piezostack to the pump body. The solution that was adopted in this case was to fill the gaps between the piezostacks and the pump body with a thermally conductive, but electrically insulating silicone compound (CHO-THERM 1642, Chomerics (2001)). Due to its extremely low shear stiffness, the compound does not affect the deformation of the piezostacks, but as a result of its large thermal conductivity, it provides an effective heat transfer path to the pump body.

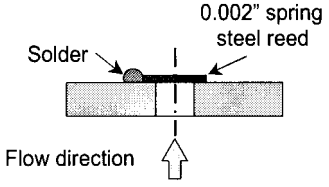

Figure 6. *Cross-sectional view of the reed valves.*

Figure 7(a) shows a test specimen used to measure the effectiveness of the passive cooling method. The test specimen represents a cross section of the piezoelectric pump, with a piezostack and the thermal compound. A strain gage was bonded to the piezostack, and the temperature of the piezostack was measured using a surface mounted thermocouple. Even though this led to the measurement of a reduced temperature than that at the core of the piezostack, the level of error was considered acceptable for the present purpose. The test specimen was excited in the same manner as the piezoelectric pump and the temperature was measured till the system reached steady state. These measurements are shown in Figure 7(b).

The piezostack temperature stabilized at approximately 70°C at an excitation frequency of 1 kHz. Since the manufacturer specified 80°C as the maximum recommended operating temperature, the maximum excitation frequency of the piezoelectric pump using passive cooling was limited to 1 kHz. The present prototype pump has a body made of steel, which has a low thermal conductivity compared to aluminum. Therefore, the steady state temperature of the piezostacks achievable by fabricating the pump body out of aluminum is expected to be lower than that of the present device.

Another approach to control the temperature of the piezostacks is by using active cooling, with Thermo-Electric Modules (TEMs). The TEMs operate off a 5 V DC supply and draw a current on the order of 1–2 A. They can be installed in the pump body with one side in contact with the piezostacks and the other side in contact with the pump body. However, the efficiency of these devices is low, and they are difficult to integrate in the pump body. For these reasons, the passive cooling scheme was implemented, and the active cooling scheme

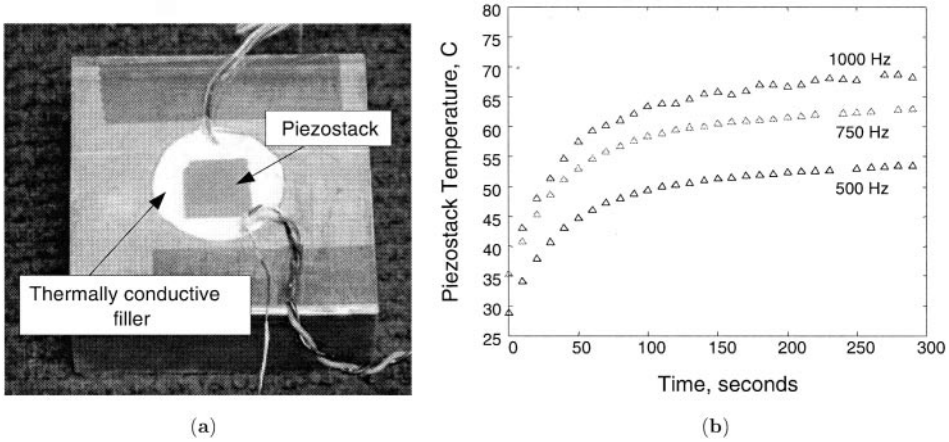

Figure 7. *Passive cooling of the piezostacks: (a) Test specimen; (b) Steady state piezostack temperatures.*

was retained as an option if more cooling is required in future tests.

Electrical Power Delivery to the Piezostacks

The delivery of electrical power to the device is an important aspect of the design. The piezostacks present a predominantly capacitive load to the power amplifier driving them. At an operating frequency of 100 Hz, the peak current drawn by the piezostacks is approximately 0.44 A. As the excitation frequency increases, supplying the large currents required would necessitate big amplifiers, effectively reducing the attractiveness of the device as a compact actuation solution (Main et al., 1996).

The first prototype piezoelectric pump was excited using a conventional linear power amplifier, (Model PA9810, roh (1999)). The PA9810 amplifier is a 700-W amplifier with a $\pm$ 500 V, $\pm$ 1.5 A output. The excitation frequency of the piezoelectric pump is limited to 300 Hz by output current limitations of the amplifier. This actuation frequency was achieved with the piezostacks connected in parallel to the amplifier output. Using two PA9810 amplifiers, one for each piezostack, the maximum excitation frequency was increased to 600 Hz.

A completely different approach of delivering power to the actuator is to recognize that the piezostacks need not be excited by a sinusoidal voltage. For a given peak displacement, as the swept volume per cycle is constant, the only parameter of consequence to the performance of the device is the frequency of excitation. Figure 8 shows the schematic circuit diagram of a piezostack driver based on this idea, that was designed and fabricated in-house. This driver will be referred to as the switched driver in subsequent discussions, and should not be confused with a switched mode power supply, or a switching power amplifier. Examples of this driving concept can be found in the device of Konishi et al. (1993, 1994) and also in various types of droplet generators, such as in inkjet printers. The circuit basically consists of two N-channel MOSFETs, labeled A and B. The piezostack is represented by a capacitance, C_p and is connected in series to the MOSFETs by a current limiting resistance, R_{LIM}. The drain of MOSFET A is connected to a DC power supply, V_{DC}, which for example, would be the DC power bus on an aircraft. Depending on the level of the control voltage, the MOSFETs exist in one of two states:

1. MOSFET A is ON and MOSFET B is OFF: In this state, the series combination of R_{LIM} and C_p is shorted to V_{DC}. The piezostack charges up to the DC bus voltage exponentially with a time constant depending on the values of R_{LIM} and C_p.
2. MOSFET A is OFF and MOSFET B is ON: In this state, the series combination of R_{LIM} and C_p is shorted to ground. The piezostack discharges exponentially with the same time constant as in the above case.

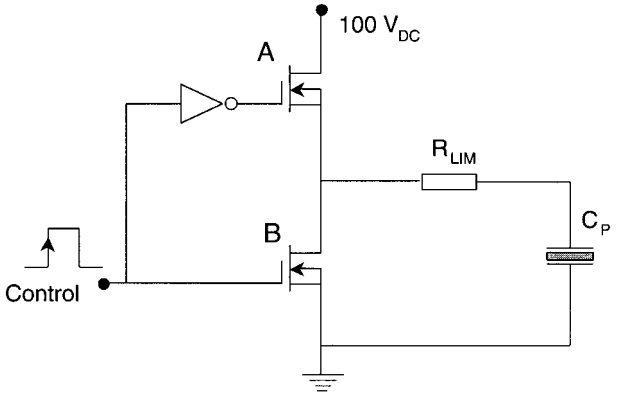

Figure 8. *Schematic of the piezostack switch driver circuit.*

As a result of the piezostack charging and discharging between states 1 and 2, the voltage appearing at the electrodes of the piezostack approximates a square wave. As the peak voltages of the sinusoidal excitation and the switched driver waveform are the same, the peak displacement of the piezostack is the same in both cases. The charging and discharging roll-offs are useful in decreasing transient loads on the piezostacks, which would otherwise respond to sharp changes in slope of the excitation voltage, creating potentially damaging internal stresses.

The main advantage of this method of exciting the piezostacks is that it is very compact. A prototype circuit was built in the lab on a circuit board with an overall footprint of less than 3 sq. in. This is mainly because the power dissipation in the driving circuit is almost zero, as a result of the low values of $R_{DS(ON)}$ of the MOSFETs. The only power that is dissipated in the circuit is in the current limiting resistance, R_{LIM}. The value of this resistance is chosen depending on the allowable peak current that can be drawn from the DC bus. The peak current is approximately given by V_{DC} / R_{LIM}.

The electrical efficiency of this method is inherently poor. However, as the primary requirement is power density of the device, the challenge in this particular application is the electric power delivery to the device. In this case, electrical efficiency is sacrificed for compactness. Using the switched driver, it was possible to test the device up to a pumping frequency of 1 kHz.

OUTPUT TEST SETUP

A test setup was fabricated to measure the output performance of the actuator. A schematic diagram of the experimental setup is shown in Figure 9. The port labeled 'Bleed' and the neighboring valves were used to fill the hydraulic circuit, aided by the application of a vacuum.

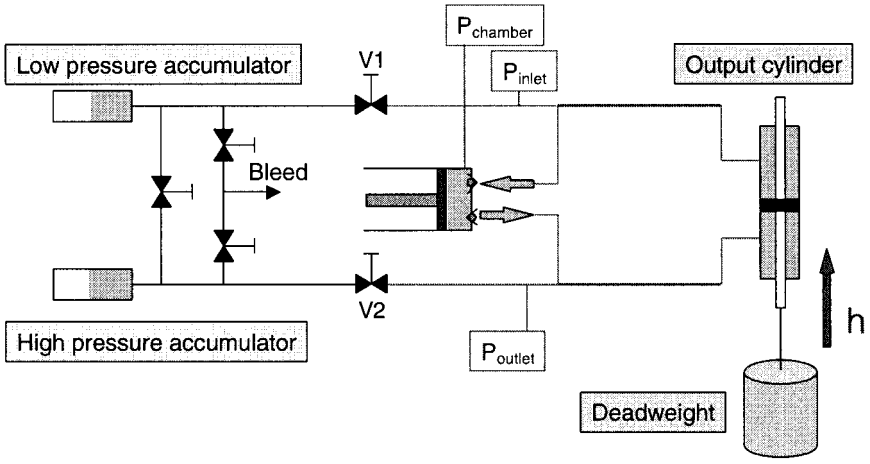

Figure 9. *Experimental setup for the evaluation of unidirectional actuator performance.*

After the fluid was filled in the circuit, a bias pressure of 50 psi was applied in order to reduce the possibility of cavitation, as well as to maintain a preload on the piezostacks. After filling the circuit, the accumulators were cut off from the rest of the circuit by means of closing valves V1 and V2. The validation of the pumping effectiveness of the piezoelectric pump, by means of creating a pressure rise between the accumulators, is described in a previous work (Sirohi and Chopra, 2001).

The fluid pressures at the inlet, outlet and pumping chamber of the piezoelectric pump are measured by pressure transducers. Each piezostack is instrumented with a strain gage in a quarter bridge configuration and the temperature of the piezostacks is measured by a thermocouple. The displacement of the output cylinder is measured with a linear potentiometer. All data acquisition was performed on a Windows NT based PC with a National Instruments PCI-6031E 16-bit DAQ card, using a virtual instrument application programmed in LabVIEW^{TM} 5.1.

EXPERIMENTAL RESULTS

Unidirectional Actuation

For the first set of experiments, only unidirectional actuation is performed, both at a no-load condition and against an external load. The external load consists of deadweights that are raised by the actuator. Output velocities are measured for each value of deadweight, as a function of pumping frequency. At the end of each test, the cylinder is manually returned to its lowest position.

Figure 10 shows the output cylinder velocity as a function of output load and driving frequency. The maximum force and the maximum no-load velocity of the actuator are approximately 35 lb and 1.2 in./s respectively. These values are in good agreement with the performance estimated in "Performance Estimations".

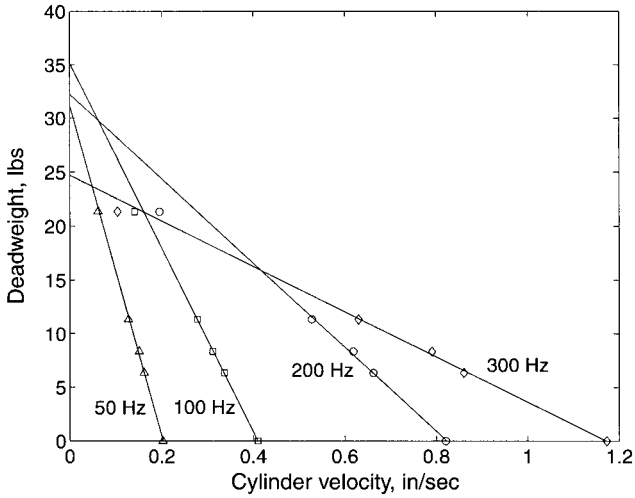

Figure 10. *Output force–velocity curves of the actuator.*

Precise measurement of the blocked force of the device is difficult. The value of blocked force is therefore obtained by fitting a straight line to the force–velocity data, and extrapolating it to the zero load condition. Consequently, the value of blocked force is highly dependent on experimental scatter and is subject to some degree of uncertainty. Theoretically, the blocked force of the device is independent of the pumping frequency, and the no-load velocity of the device is linearly proportional to the pumping frequency. However, in the present experiment, the load mass is lifted through a finite distance during each pumping cycle. The inertia forces resulting from these accelerations of the load mass result in a decrease in output force of the device with pumping frequency. From Figure 10, it can be seen that the blocked force is slightly different for pumping frequencies of 50 Hz and 100 Hz. This difference is largely due to the experimental scatter. However, the decrease in output force capability due to the effect of inertia loading is more apparent in the case of the higher pumping frequencies, 200 and 300 Hz.

Figure 11 shows the measured pumping chamber force–displacement curves for several output deadweights, at a pumping frequency of 50 Hz and a bias pressure of 50 psi, superimposed on the effective piezostack load line. It can be seen that the shape of the pressure traces follows the theoretical parallelogram shape quite closely at the relatively low pumping frequency of 50 Hz. The effect of fluid compressibility can also be seen from the figure. The measured value of fluid compressibility agrees well with the estimated value as given by Equation (13).

Figure 12 shows a comparison of the output cylinder velocity with Type I and Type II valves, upto a pumping frequency of 600 Hz. In this case, the piezostacks were excited with two PA9810 amplifiers. The errorbars on the plots show the amount of experimental scatter in the data. As expected, for a given load condition, the Type II valves with a higher natural frequency show a larger flow rate than the Type I valves. For the maximum tested deadweight of 11.34 lb, at a pumping frequency of 300 Hz, the Type II valves permit approximately 1.5 times larger flow rate than the Type I valves. Therefore, it can be concluded that the Type II valves are more suited to high pumping frequencies than the Type I valves.

To investigate the effect of even higher pumping frequencies, the actuator was excited with the switched driver up to a frequency of 1 kHz. The no-load flow rates as a function of pumping frequency up to a frequency of 1 kHz is shown in Figure 13. The dip in the output velocity at around 500 Hz is believed to be caused by the dynamics of the hydraulic circuit and tubing. Investigation of these dynamics is the next step in order to increase the pumping efficiency at high frequencies.

Bidirectional Actuation

For realistic applications, bidirectional operation of the output cylinder is necessary. Therefore, after completion of the output power experiments with unidirectional actuation, a 4-way valve was incorporated in the

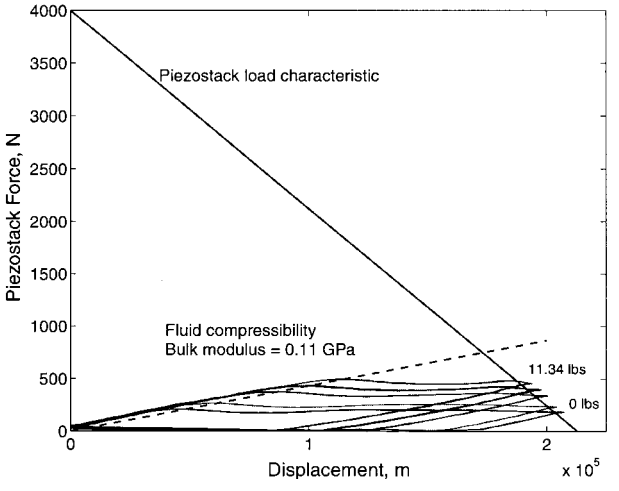

Figure 11. *Measured pumping chamber force–displacement curves, for 50 Hz pumping frequency, and 50 psi bias pressure.*

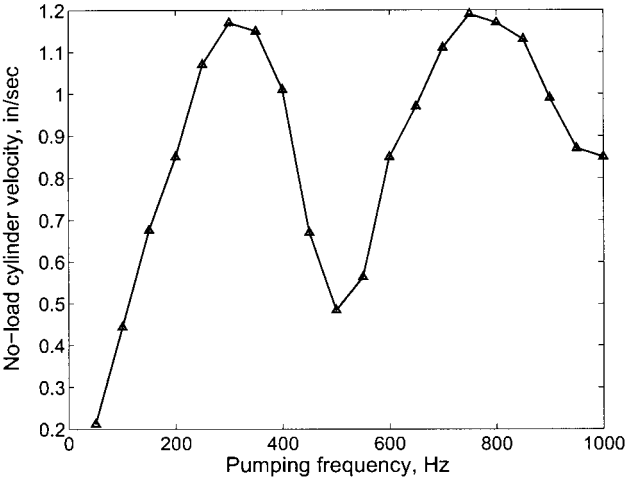

Figure 13. *No-load cylinder velocities upto 1 kHz pumping frequency, Type II valves.*

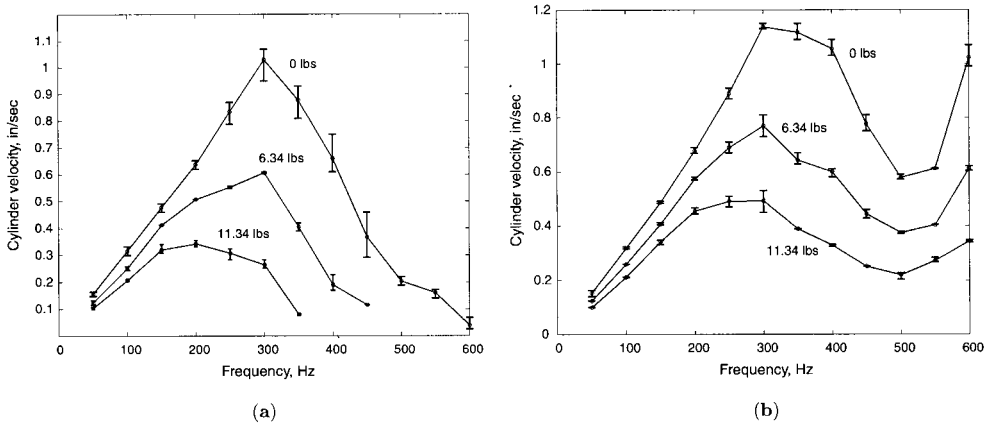

Figure 12. *Output cylinder velocity as a function of load and pumping frequency, 50 psi bias pressure: (a) Type I valves; (b) Type II valves.*

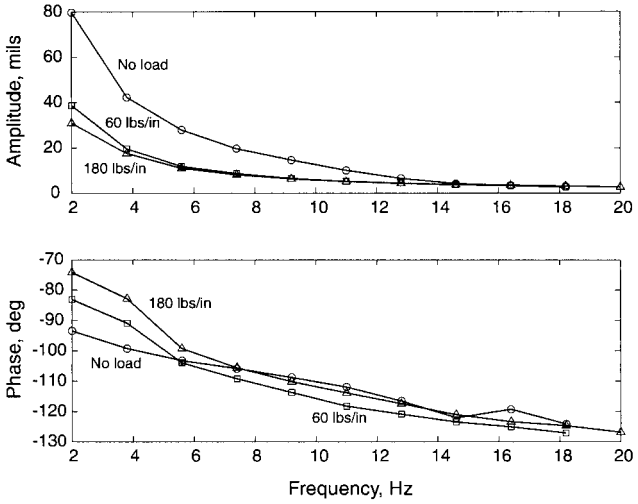

Figure 14. *Output cylinder stroke as a function of output frequency, with external spring load, at 300 Hz pumping frequency.*

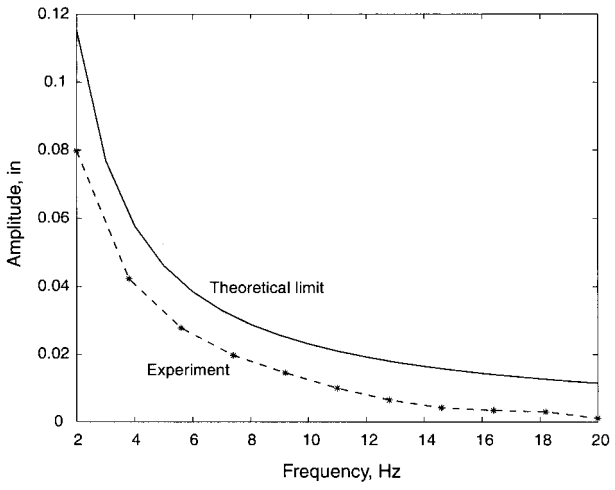

Figure 15. *Correlation of measured no-load output displacement with predicted value at 300 Hz pumping frequency.*

circuit between the piezoelectric pump and the hydraulic cylinder. The 4-way valve was a commercially available spool valve (HR Textron Model 27A50 R-DDV, HR Textron (2000)), with a bandwidth of approximately 200 Hz.

Measurement of bidirectional actuation performance was performed under no-load and spring loaded conditions. The spring load consisted of a cantilevered beam with its tip connected to the output of the actuator. Experiments were performed with two different spring stiffnesses, of approximately 60 and 180 lb/in. The external load was chosen to be of a purely spring type, with no deadweight, so that there would be no bias force acting on the actuator. As all the testing was open loop, a bias force would have caused the output displacement to drift.

A stepped sinusoidal voltage of amplitude 5 V, at a frequency ranging from 2 to 20 Hz was input to the 4-way valve. The pump was operated at a constant frequency of 300 Hz, at 0–100 V. The amplitude and phase of the output displacement of the actuator is plotted in Figure 14. It should be noted that for the frequency range considered, the dynamics of the 4-way valve is not significant. At a frequency of 5 Hz, the amplitude of the output displacement was measured to be 32 mils under no external load, dropping to 15 mils under an external spring load of 180 lb/in.

A theoretical limiting curve for output displacement amplitude as a function of output frequency is obtained using the no-load unidirectional velocity data plotted in Figure 12(b). This is compared to the experimentally measured output displacement amplitudes, at a pumping frequency of 300 Hz, in Figure 15. It can be seen that the shapes of both curves are quite identical, whereas the experimental data are lower by a constant offset of approximately 0.03 in. This is attributed to the leakage in the 4-way valve.

SUMMARY AND CONCLUSIONS

The basic motivation for developing the piezoelectric–hydraulic hybrid actuation concept is to increase the energy density of actuators based on the frequency rectification of piezoceramic stacks, which relies on the conversion of a small stroke, high frequency input to a larger stroke, lower frequency output. Therefore, in order to increase the output power, it is important to have as high an input frequency as possible. Several actuators based on this concept have been recently developed; however, they are mostly based on large piezostacks operating at relatively low frequencies. The present work focuses on a piezostack driven pump operated at a high frequency and low per cycle volumetric displacement. The actuator under development in the present study is envisaged as a potential actuator for a trailing edge flap on a smart rotor system.

Several major challenges exist to operating the actuator at high pumping frequencies. These issues, along with the solutions implemented in the present prototype in order to achieve a maximum pumping frequency of 1 kHz are discussed below:

1. Frequency response of the passive check valves: Approximately 30% larger flow rates at high pumping frequencies were achieved using the high natural frequency Type II (reed) passive check valves as opposed to the commercially available Type I ball type valves. From measurements of the output flow rates, as well as pressure traces in the pumping chamber of the pump, it can be concluded that the Type II valves are better suited for high frequency pumping.
2. Self-heating of the piezostacks: Keeping the temperature of the piezostacks under 80°C is imperative according to the manufacturers' specifications. This is achieved in the current design using a passive

method to conduct heat away from the piezostacks. This results in a steady state piezostack temperature of approximately 70°C at a pumping frequency of 1 kHz.

3. Electrical power delivery to the piezostacks: Large power amplifiers are required to supply a high frequency sinusoidal excitation to the piezostacks. In the present design, the piezostacks were driven by a compact switched driver, that was designed and fabricated in-house and which enabled excitation of the piezostacks upto 1 kHz. It should be noted that in the present design, the maximum excitation frequency of 1 kHz was limited not by electrical power delivery issues, but by the maximum temperature of the piezostacks as a result of self-heating.

The present actuator was operated by two piezostacks of a total length of 36 mm and cross-sectional area 100 mm^2, upto a pumping frequency of 1 kHz. However, the maximum fluid flow rate was observed at a pumping frequency of approximately 300 Hz. Unidirectional actuation of the output hydraulic cylinder yielded a no-load cylinder velocity of approximately 1.2 in/s and a blocked force of 35 lbs. Under bidirectional actuation, a no-load displacement amplitude of 32 mils was measured at 5 Hz, dropping to 15 mils under a spring load of 180 lb/in. The introduction of the 4-way valve in the hydraulic circuit resulted in a loss of output displacement of approximately 20% due to internal leakage. The no-load output displacement amplitude drops to 12 mils at a frequency of 10 Hz. It can be concluded that in its present form, the prototype actuator is more suited for quasi-static applications, involving a long output stroke at a low frequency, as opposed to oscillatory output at a short stroke and high frequency. It is envisaged that a better understanding of the dynamics of the hydraulic circuit would result in an improvement in the pumping effectiveness at high frequencies, enabling an increase in the bandwidth of the actuator.

FUTURE WORK

In order to better understand the dynamics of the hydraulic tubing and fluid, and possibly utilize these effects to increase the output flow rate of the device, a detailed analytical model of the device including valve dynamics, hydraulic circuit dynamics, and fluid inertia needs to be developed and validated. An increase in the output stroke and bandwidth is only possible by increasing the flow rate of the pump. Future research efforts should focus on increasing the flow rate of the pump at high frequencies.

The issue of electrical power delivery, which is one of the major obstacles to high frequency pumping operation, was addressed in the present research by means of actuating the piezostacks with the switched driver. However, the long term effects of actuating the piezostack in this manner, with respect to fatigue failure, has not been addressed. This would be of considerable importance in a real application and should be investigated in future research.

The maximum pumping frequency of 1 kHz was dictated by temperature limits of the piezostacks. In future devices, a careful design of heat transfer mechanisms is necessary. For example, construction of the pump body out of aluminum would reduce the steady state temperature of the piezostacks for the same frequency excitation. The possibility of integrating TEMs in the pump body should also be evaluated in the event of insufficient passive heat transfer.

Bidirectional output of the device is achievable only through the use of a 4-way valve installed on the output of the piezoelectric pump. However, the smallest conventional 4-way valves are almost as big as the piezoelectric pump itself, effectively reducing the power density of the device by almost half. Additionally, leakage in the 4-way valve results in a decrease in the effective flow rate. This is a major limitation of the present design, and future efforts should be directed toward active check valves, that would perform both the functions of the passive check valves and the 4-way valve.

ACKNOWLEDGMENTS

The authors would like to acknowledge CSA Engineering Inc., and DARPA for their support. Useful discussions with Dr. Jinhyeong Yoo, Dr. Chris Cadou, Dr. Eric Anderson, and Jason Lindler are also gratefully acknowledged.

REFERENCES

1997. Products for Micropositioning, US-Edn., Physik Instrumente (PI).

1997. *Technical Hydraulic Handbook*, The Lee Company.

1999. "HERO precision power amplifier, model PA9810," ROHRER Meβ und Systemtechnik; e-mail: rohrer@online.de, Munich, Germany, Technical Manual.

2000. "Hydraulic R-DDV Servovalves," HR Textron, 25200 W. Rye Canyon Road, Santa Clarita, CA 91355, http://www.hrtextron.com.

2001. "Thermal Management Products Catalog," Chomerics North America; Parker Hannifin Corporation, 77 Dragon court, Woburn MA 01888-4014, http://www.chomerics.com.

Gerver, M.J., Goldie, J.H. Swenbeck, J.R.., Shea, R., Jones, P., Ilmonen, R.T., Dozor, D.M., Armstrong, S., Roderick, R., Nimblett, F.E. and Iovanni, R. 1998. "Magnetostrictive Water Pump." In: *Proceedings of the 6th SPIE Conference on Smart Structures and Integrated Systems*, Vol. 3329, Newport Beach, C.A, pp. 694–705.

Konishi, K., Yoshimura, T., Hashimoto, K., Hamada, T. and Tamura, T. 1994. "Hydraulic Actuators Driven by Piezoelectric Elements(2nd Report. Enlargement of Piezoelectric Pumps Output Power Using Hydraulic Resonance)," *Journal of Japanese Society of Mechanical Engineering* (*C*), 60(571):228–235.

Konishi, K., Yoshimura, T., Hashimoto, K. and Yamamoto, N. 1993. "Hydraulic Actuators Driven by Piezoelectric Elements(I Report., Trial Piezoelectric Pump and its Maximum Power)," *Journal of Japanese Society of Mechanical Engineering* (*C*), 59(564): 213–220.

Lee, T. and Chopra, I. 2001. "Design of Piezostack-driven Trailing-edge Flap Actuator for Helicopter Rotors," *Smart Materials and Structures*, 10(1):15–24.

Main, J.A., Newton, D.V., Massengill, L. and Garcia, E. 1996. "Efficient Power Amplifiers for Piezoelectric Applications," *Smart Materials and Structures*, 5(6):766–775.

Mauck, L.D. and Lynch, C.S. 2000. "Piezoelectric Hydraulic Pump Development," *Journal of Intelligent Material Systems and Structures*, 11:758–764.

Mauck, L.D., Oates, W.S. and Lynch, C.S. 2001. "Piezoelectric Hydraulic Pump Performance." In: *Proceedings of the 8th SPIE Conference on Smart Structures and Materials*: *Industrial and Commercial Applications of Smart Structures Technologies*, Vol. 4332, Newport Beach, CA, pp. 246–253.

McCloy, D. and Martin, H. 1980. *Control of Fluid Powrer*: *Analysis and Design*, Ellis Horwood Limited, Chichester, England, Second(revised) edition.

Nasser, K., Leo. D.J. and Cudney, H.H. 2000. "Compact Piezohydraulic Actuation System." In: *Proceedings of the 7th SPIE Conference on Smart Structures and Integrated Systems*, Vol. 3991, Newport Beach, CA, pp. 312–322.

Sirohi, J. and Chopra, I. 2001. "Development of a Compact Piezoelectric-Hydraulic Hybrid Actuator." In: *Proceedings of the 8th SPIE Conference on Smart Structures and Integrated Systems*, Vol. 4327, Newport Beach, CA, pp. 401–412.

Sirohi, J. and Chopra, I. 2002. "Design and Testing of a High Pumping Frequency Piezoelectric-Hydraulic Hybrid Actuator." In: *Proceedings of the 9th. SPIE Conference on Smart Structures and Integrated Systems*, San Diego, CA.